Journal of Solid State Chemistry **163,** 267–274 (2002)
doi:10.1006/jssc.2001.9406, available online at http://www.idealibrary.com on IDEAL®

An Electron Diffraction and XRPD Study of Superlattice Ordering in the Elpasolite-Related Oxyfluoride $K_3MoO_3F_3$

F. J. Brink,*,[1] R. L. Withers,*,[2] K. Friese,† G. Madariaga,† and L. Norén*

*Research School of Chemistry, Australian National University, Canberra, ACT 0200, Australia; and †Departamento de Fisica de la Materia Condensada, Universidad del Pais Vasco, Bilbao, E-48080, Spain

Received July 2, 2001; in revised form September 14, 2001; accepted September 21, 2001

A detailed electron diffraction and XRPD study has been made of the room-temperature α polymorph of $K_3MoO_3F_3$. It is shown that the true symmetry of this polymorph is neither tetragonal, trigonal, nor triclinic as previously reported but rather monoclinic $I1a1$, $a = 2a_p - c_p$, $b = 4b_p$, $c = a_p + 2c_p$ when expressed in terms of the underlying elpasolite (ordered perovskite) parent structure type. A highly structured, three-dimensional, continuous diffuse intensity distribution (presumably arising from local O/F ordering and associated structural relaxation) is shown to coexist with the sharp satellite reflections characteristic of the monoclinic supercell. © 2002 Elsevier Science

INTRODUCTION

An extremely widespread group of compounds, including halides, oxides, sulfides, nitrates, and cyanides as well as oxyfluorides, are known to crystallize either in the ideal cubic ($Fm\bar{3}m$) A_2BMX_6 elpasolite (ordered perovskite) structure type (see Fig. 1) or in closely related displacive variants thereof (1–4). $K_3MoO_3F_3$ is one member of the rather large subgroup of oxyfluoride phases ($A_2^+B^+M^{IV}OF_5$ (A, B = an alkali ion; M^{IV} = Ti, V), $A_2^+B^+M^{V}O_2F_4$ (A, B = alkali; M^{V} = V, Nb), and $A_2^+B^+M^{VI}O_3F_3$ (A, B = K, Rb, Cs; M^{VI} = Mo, W)) (3, 4) which belong to this group. Despite the two chemically distinct anion species in the case of the latter oxyfluoride subgroup, there has to date been no evidence for oxygen/fluorine ordering in any of these phases (as is also the case for many other oxyfluoride systems (5)); i.e., random anion site disorder has invariably been reported for the anion, or X, site positions (3, 6).

Like many elpasolite-related phases (1–3), the ideal cubic ($Fm\bar{3}m$) structure (see Fig. 1) is not the structure of the room-temperature polymorph of $K_3MoO_3F_3$ but rather that of its highest temperature polymorph (6–11). $K_3MoO_3F_3$ undergoes a series of reversible structural phase transitions on cooling from this high-temperature ideal cubic polymorph. The typical transition sequence for the $A_2^+B^+M^{VI}O_3F_3$ (A, B = K, Rb, Cs; M^{VI} = Mo, W) family of elpasolite-related phases (6–11), particularly when the A and B cations are of the same type (9), is from a highest temperature, ideal cubic ($Fm\bar{3}m$) γ polymorph (above T_2) through an intermediate (ferroelectric and also reported to be ferroelastic) β polymorph ($T_1 < T < T_2$) to a low-temperature (ferroelectric as well as ferroelastic) α polymorph (below a transition temperature T_1 which is usually above room temperature). (In the case of $K_3MoO_3F_3$ these transition temperatures correspond to $T_1 = 436$ K and $T_2 = 522$ K, respectively (9)).

Pausewang and Rüdorff (3) initially reported the symmetry of $K_3MoO_3F_3$ at room temperature (i.e., in the low-temperature α polymorph) to be, in all probability, orthorhombic or monoclinic albeit with tetragonal metric symmetry. The (body-centered) tetragonal unit cell (subscript q) reported therein (3) (corresponding to $\mathbf{a}_q = \frac{1}{2}(\mathbf{a}_p + \mathbf{b}_p)$, $\mathbf{b}_q = \frac{1}{2}(-\mathbf{a}_p + \mathbf{b}_p)$, $\mathbf{c}_q = \mathbf{c}_p$ when indexed with respect to the parent $Fm\bar{3}m$ unit cell (subscript p)) does not expand the size of the primitive parent unit cell and hence does not imply the existence of satellite reflections in addition to the strong Bragg reflections, $\mathbf{G}_p$, of the underlying parent structure.

Subsequently, however, Péraudeau *et al.* (7–9) did discover weak satellite reflections in the low-temperature α polymorph which apparently disappeared on heating above T_1 and which do require the existence of a long period supercell. This is rather unusual for elpasolites where most structural phase transitions have experimentally been found to be connected with relatively simple octahedral tilt patterns and/or shifts of the A cations (1, 2) which almost invariably do not significantly expand the size of the parent unit cell. Indexation of the XRD patterns of the various low-temperature α polymorphs was reported by Péraudeau *et al.* (7–9) to give rise to a large tetragonal

[1] Also at Electron Microscope Unit, Research School of Biological Sciences, Australian National University, Canberra, ACT 0200, Australia

[2] To whom correspondence should be addressed.

0022-4596/02 $35.00
© 2002 Elsevier Science
All rights reserved.

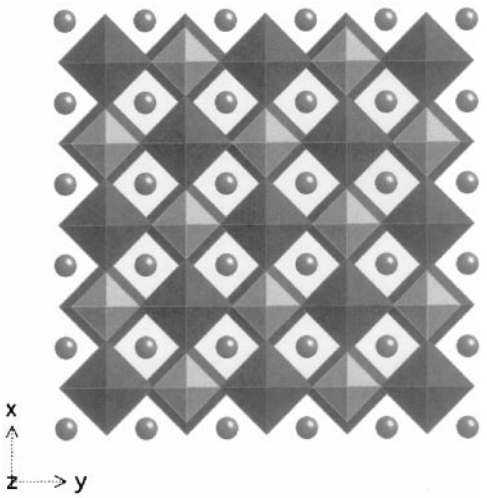

FIG. 1. Schematic $\langle 001 \rangle$ projection of the ideal cubic ($Fm\bar{3}m$) A_2BMX_6 elpasolite parent structure type. The BX_6 (dark and larger) and MX_6 (gray and smaller) (A = anion) octahedra are shown hatched. The A cations are represented by the gray balls.

supercell (subscript Q) corresponding to $\mathbf{a}_Q = 5\mathbf{a}_q = \frac{5}{2}(\mathbf{a}_p - \mathbf{b}_p)$, $\mathbf{b}_Q = 5\mathbf{b}_q = \frac{5}{2}(\mathbf{a}_p + \mathbf{b}_p)$, $\mathbf{c}_Q = 5\mathbf{c}_q = 5\mathbf{c}_p$ with matching reciprocal space unit cell vectors $\mathbf{a}_Q^* = \frac{1}{5}\mathbf{a}_q^* = \frac{1}{5}[110]_p^*$, $\mathbf{b}_Q^* = \frac{1}{5}\mathbf{b}_q^* = \frac{1}{5}[\bar{1}10]_p^*$, and $\mathbf{c}_Q^* = \frac{1}{5}\mathbf{c}_q^* = \frac{1}{5}[001]_p^*$. Thus, satellite reflections should be observed at $\mathbf{G}_p \pm \frac{J}{5}\langle 110\rangle_p^* \pm \frac{K}{5}\langle 001\rangle_p^*$; J,K are integers, $\mathbf{G}_p$ is a parent Bragg reflection if this supercell reported by Péraudeau *et al.* (7–9) is correct.

Matters were subsequently complicated still further when both Ravez *et al.* (10) and Abrahams *et al.* (6) reported that the intermediate β polymorph (of $Rb_2KMoO_3F_3$) actually had rhombohedral (rather than tetragonal) point group symmetry and that the most probable point group symmetry of the α polymorph below T_1 was either trigonal or triclinic (but again not tetragonal). More recently still, Ye *et al.* (11) in an optical and dielectric study of apparent single crystals of $K_3MoO_3F_3$ reported a ferroelastic domain structure (visible by polarized light microscopy) in both α and β polymorphs apparently consistent only with trigonal symmetry. The unchanged nature of the ferroelastic domain walls on passing through T_1 led these authors to conclude that "…the α to β phase transition at T_1 takes place between trigonal symmetries…". Furthermore, as a result of the dependence of the discontinuity of the birefringence at T_1 on the heating or cooling rate, these authors suggested that the α to β phase transition "…is probably of incommensurate nature…." No direct diffraction evidence for the existence of incommensurate satellite reflections in the low-temperature α polymorph, however, was reported.

Given the confusion in the literature outlined above in conjunction with the known ability of electron diffraction to resolve problems associated with pseudosymmetry and twinning, it was decided to undertake a combined electron diffraction and XRPD study of the unit cell and space group symmetry of the lower temperature α polymorph of $K_3MoO_3F_3$—a representative member of the $A_2^+B^+M^{VI}O_3F_3$ (A, B = K, Rb, Cs; M^{VI} = Mo, W) family of elpasolite-related oxyfluoride phases. The purpose of the current contribution is to present the results of this study and this work is part of a wider search for diffraction evidence of oxygen/fluorine ordering in oxyfluoride systems.

EXPERIMENTAL

The $K_3MoO_3F_3$ used in this study was prepared by the reaction of a 1:3 molar ratio of MoO_3 (Halewood Chemicals Ltd., 99.999%) with KF (Aldrich, 99%, spray-dried) in a sealed platinum tube at 600°C for 36 hrs. All reactants were manipulated in a dry box under dry argon to minimize contamination with air or water vapor. XRD data collected from a Guinier-Hägg camera ($\lambda = 1.5406$ Å), using an internal Si (NBS #640) standard, were used for phase analysis and to refine unit cell parameters. Samples suitable for transmission electron microscope (TEM) work were prepared by the dispersion of finely ground material onto a holey carbon film. Electron diffraction patterns (EDPs) were obtained, using both conventional negatives as well as more sensitive imaging plates (Micron-Ditabis), on a Philips EM 430 TEM.

RESULTS

Electron Diffraction Results—Long-Range Order

Figure 2a shows a typical $\langle 001\rangle_p$ type zone axis electron diffraction pattern (EDP) of the α polymorph of $K_3MoO_3F_3$. In addition to the strong Bragg reflections of the underlying parent structure (labelled $\mathbf{G}_p$ in what follows), note the existence of $\mathbf{G}_p \pm \frac{J}{5}\langle 420\rangle_p^*$ (J is an integer) type superlattice reflections running along both the $[402]_p^*$ and $[40\bar{2}]_p^*$ directions of reciprocal space. The tetragonal supercell ($\mathbf{a}_Q = \frac{5}{2}(\mathbf{a}_p - \mathbf{b}_p)$, $\mathbf{b}_Q = \frac{5}{2}(\mathbf{a}_p + \mathbf{b}_p)$, $\mathbf{c}_Q = 5\mathbf{c}_q = 5\mathbf{c}_p$; $a_Q = 30.61$, $c_Q = 43.61$ Å) proposed by Péraudeau *et al.* (7–9) for this room-temperature α polymorph also implies the existence of satellite reflections, but running along the $\langle 110\rangle_p^*$ and $\langle 001\rangle_p^*$ directions of reciprocal space (at $\mathbf{G}_p \pm \frac{J}{5}\langle 110\rangle_p^* \pm \frac{K}{5}\langle 001\rangle_p^*$; J,K are integers, etc. - see above) rather than the observed $\langle 420\rangle_p^*$ directions of reciprocal space. The fact that satellite reflections of this type were never observed means that the proposed tetragonal supercell of Péraudeau *et al.* (7–9) is incorrect and can be ruled out.

In general, whenever more than one set of $\mathbf{G}_p \pm \frac{J}{5}\langle 420\rangle_p^*$ type reflections are excited at any one particular zone axis orientation, then satellite reflections are also observed to run along that direction (see, for example, Figs. 2a and 3a), i.e., twinning attempts to restore the $m\bar{3}m$ point group symmetry of the underlying parent structure. By careful

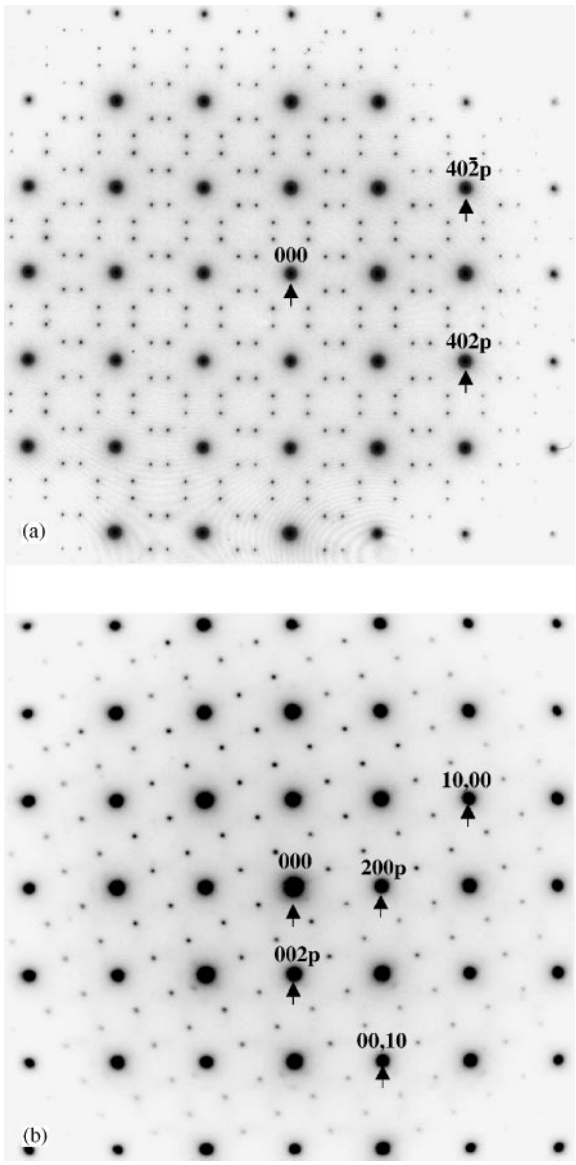

FIG. 2. (a) A typical twinned $\langle 010\rangle_p$ type zone axis EDP of the α polymorph of $K_3MoO_3F_3$. In addition to the strong Bragg reflections of the underlying parent structure (subscript p), note the existence of $\mathbf{G}_p \pm \frac{J}{5}\langle 420\rangle_p^*$ (J is an integer) type superlattice reflections running along both the $[402]_p^*$ and $[40\bar{2}]_p^*$ directions of reciprocal space. (b) The equivalent single domain $\langle 010\rangle_p$ type zone axis EDP in which only $\mathbf{G}_p \pm \frac{J}{5}[40\bar{2}]_p^*$ superlattice reflections are locally present. Indexation with a subscript p is with respect to the underlying parent structure while indexation without the subscript p is with respect to the resultant monoclinic supercell.

positioning of the electron probe on the particular grain being investigated, however, it is usually possible to observe a significant weakening, if not disappearance, of one or the other set of $\mathbf{G}_p \pm \frac{J}{5}\langle 420\rangle_p^*$ superlattice reflections (cf., for example, Fig. 2b with 2a and Fig. 3b with 3a; note that $\frac{1}{5}[351]_p^* \equiv [111]_p^* - \frac{1}{5}[204]_p^*$ etc. in Fig. 3). The implication is that only one independent set of $\mathbf{G}_p \pm \frac{J}{5}\langle 420\rangle_p^*$ superlattice reflections exists in any one single domain, nontwinned area. This rules out the possibility of the resultant unit cell having trigonal symmetry as proposed by Ye *et al.* (11).

That the apparent 4*mm* symmetry of Fig. 2a arises as a result of twinning is clear from Fig. 2b which shows a single domain $\langle 001\rangle_p$ type zone axis EDP in which only $\mathbf{G}_p \pm \frac{J}{5}[40\bar{2}]_p^*$ (or equivalently $\mathbf{G}_p \pm \frac{J}{5}[204]_p^*$) superlattice reflections are locally present; i.e., the primary mirrors perpendicular to $\mathbf{a}_p$ and $\mathbf{c}_p$ (of the $Fm\bar{3}m$ parent structure) as well as the relevant $\langle 101\rangle_p$ tertiary mirrors are also clearly broken locally. A rather more subtle breaking of symmetry arises from the fact that the magnitude of c_p^* is reproducibly

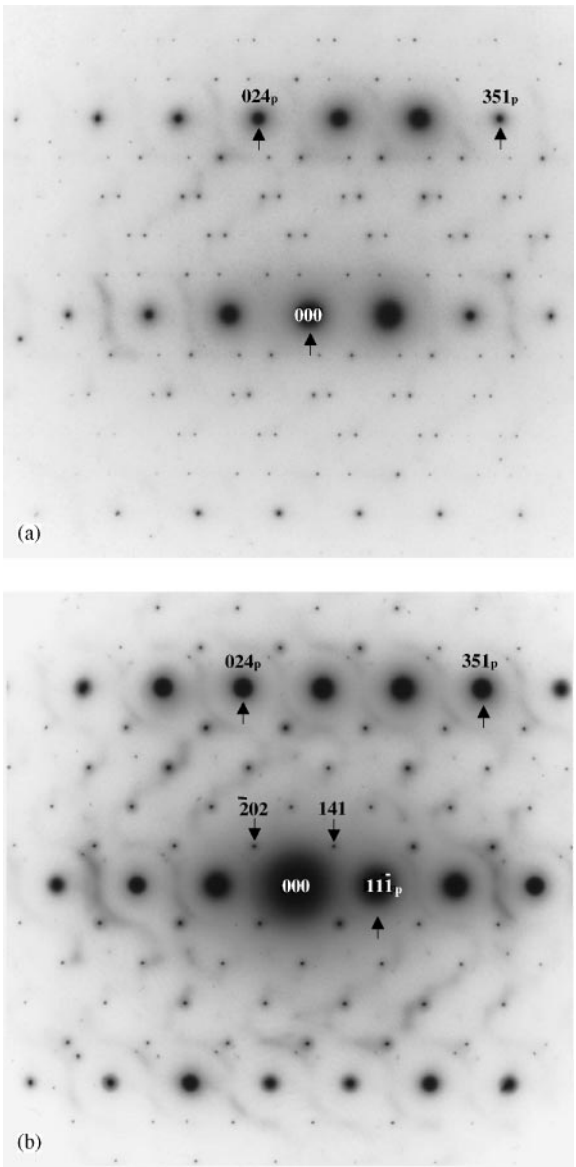

FIG. 3. (a) A twinned $\langle 3\bar{2}1\rangle_p$ type zone axis EDP. (b) The corresponding single domain EDP. Indexation with a subscript p is again with respect to the underlying parent structure while indexation without the subscript p in (b) is with respect to the resultant monoclinic supercell.

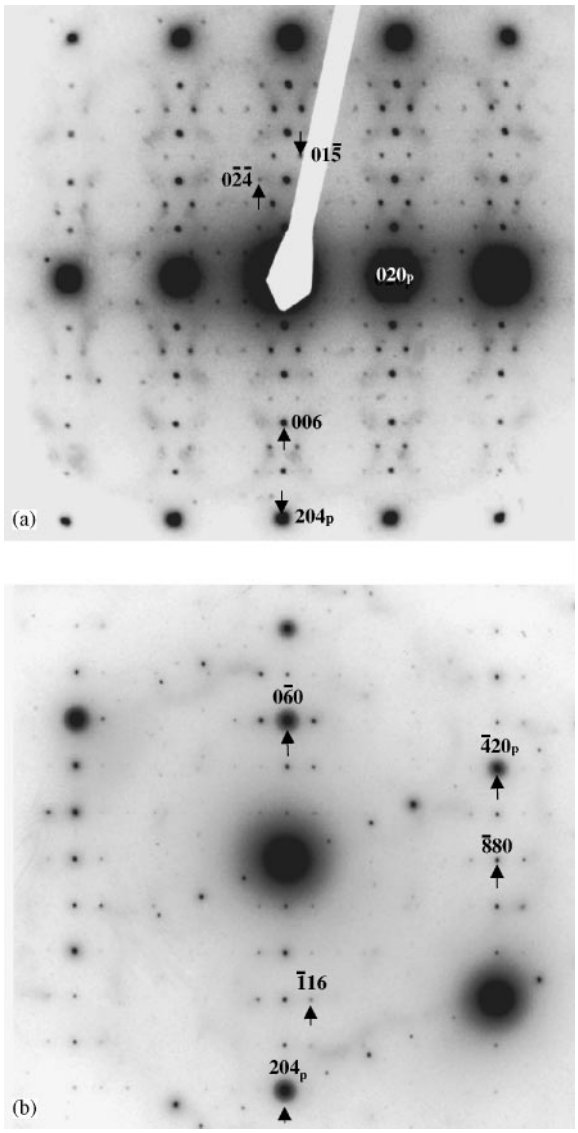

FIG. 4. (a) A (single domain) $[40\bar{2}]_p$ ($\equiv$ [100] supercell) zone axis EDP orthogonal to Fig. 2b. (b) A $[24\bar{1}]_p$ ($\equiv$ [110] supercell) zone axis EDP.

$\sim$1% less than that of a_p^*, as is apparent from careful measurement of EDPs such as that shown in Fig. 2b. (XRPD gives two distinct $\langle 002\rangle_p^*$ lines split by $\sim$0.7%, see below). The point group symmetry of Fig. 2b is thus only 2 and not the apparent 4. This confirms that both tetragonal and trigonal resultant symmetry can be ruled out for the α polymorph.

Figure 4a shows a (single domain) $\langle 40\bar{2}\rangle_p$ zone axis EDP orthogonal to Fig. 2b. The existence of satellite reflections of the form $\mathbf{G}_p + \frac{J}{10}\langle 204\rangle_p^* + \frac{K}{8}\langle 020\rangle_p^*$ when $J + K$ is even is immediately apparent. Taken in conjunction with Fig. 2b, the implied resultant reciprocal space unit cell is given by $\mathbf{a}^* = \frac{1}{10}[40\bar{2}]_p^*$, $\mathbf{b}^* = \frac{1}{8}[020]_p^*$, $\mathbf{c}^* = \frac{1}{10}[204]_p^*$. Indexation without the subscript p in Figs. 2–4 is with respect to this reciprocal space unit cell. The corresponding real space unit cell is given by $\mathbf{a} = 2\mathbf{a}_p - \mathbf{c}_p$, $\mathbf{b} = 4\mathbf{b}_p$, $\mathbf{c} = \mathbf{a}_p + 2\mathbf{c}_p$. Figure 4b shows a [110] zone axis EDP when indexed with respect to this supercell. (The satellite reflections running along the $[\bar{4}20]_p^*$ direction in Fig. 4b are attributed to a second twin domain.) The observed extinction conditions when indexed with respect to this cell are given by $F(hkl) = 0$ unless $h + k + l$ is even (see Figs. 2–4) and $F(h0l) = 0$ unless h and l are both even (see Fig. 2b). The only space groups compatible with these observed extinction

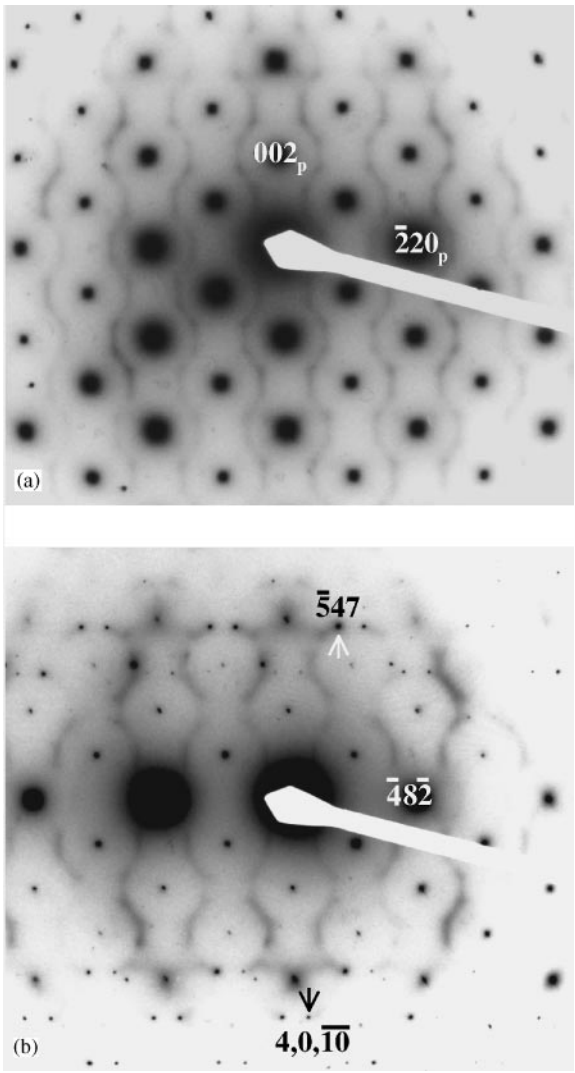

FIG. 5. (a) A typical $\langle 110\rangle_p$ zone axis EDP showing the fascinating continuous sinusoidal diffuse intensity distribution characteristic of the α polymorph of $K_3MoO_3F_3$. (b) A close to $\langle 110\rangle_p$ zone axis EDP obtained by tilting off by $\sim 3.5^\circ$ around the systematic row of (a) in order for some of the satellite reflections, such as those arrowed, to be excited in the zero order Laue zone (ZOLZ). Note that the supercell satellite reflections in this EDP condense out upon the continuous diffuse distribution, suggesting that the structural origins of the two diffraction phenomena are somehow intimately linked.

conditions are monoclinic $I1a1$ or $I12/a1$. There is, however, no inversion symmetry as the α polymorph is known to be ferroelectric (6–11). The resultant space group is therefore uniquely determined to be monoclinic $I1a1$ (a nonstandard setting of space group no. 9, Cc). X-ray diffraction results (precession photographs, etc.) from a nominal "single crystal" are consistent with the above electron diffraction determined unit cell and space group symmetry.

Given the 48 point group symmetry operations of the $m\bar{3}m$ parent structure and the 2 point group symmetry operations of the $1m1$ resultant structure, it is clear that there are 24 possible orientation variants (twins) of the final resultant structure. In conjunction with the tetragonal (very nearly cubic) metric symmetry (see below), it is not surprising that twinning is ubiquitous and often difficult to detect, and the growth of nontwinned single crystals is virtually impossible.

Electron Diffraction Results—"Short-Range" Order

In addition to the sharp satellite reflections described above, the keen observer will already have noticed the presence in some EDPs (see Figs. 3b and 4a) of a weak but characteristically shaped diffuse intensity distribution upon which, or at least very close to which, some of the satellite reflections appear to have condensed. At first it was thought that the β to α phase transition might be associated with this condensation process and that the apparent presence of the diffuse distribution at room temperature might be due to electron-beam-induced radiation damage (for which there is some evidence, see below). In this scenario, the diffuse distribution should exist in the β phase but disappear in the α phase as happens, e.g., for the "disordered" to ordered phase transition in Co_3Sn_2 (12).

Repeated observations on fresh grains (see Figs. 5 and 6), however, make it clear that the diffuse distribution does not disappear at the β to α phase transition and truly coexists with the sharp satellite reflections in the α phase (à la, e.g., $Ca_5Y_4S_{11}$ (13)). Figure 5b, for example, shows a close to $\langle 110\rangle_p$ zone axis EDP (tilted off by $\sim 3.5^\circ$ around the $\bar{2}20_p$ systematic row in order for some of the satellite reflections, such as those arrowed, to be excited in the zero order Laue zone, or ZOLZ) showing the coexistence of the satellite reflections and a fascinating continuous diffuse distribution very reminiscent of the diffuse scattering typical of the family of substoichiometric transition metal carbides and nitrides at $\langle 110\rangle$ zone axis orientations (14). Note that the satellite reflections in this EDP condense out upon the continuous diffuse distribution, suggesting that the structural origin of the two diffraction phenomena are somehow intimately linked. Figure 5a shows the corresponding diffuse distribution at the exact $\langle 110\rangle$ zone axis orientation. Comparison of Fig. 5a with Fig. 5b shows that the shapes of two-dimensional sections through the three-dimensional continuous diffuse distribution are clearly rather sensitive to the exact zone axis orientation.

In most situations, however, the relative intensity of the diffuse distribution to the parent Bragg reflections is typically rather weak, making it difficult to obtain good quality EDPs of the diffuse. Increasing the exposure time dramatically simply saturated the electron film. Imaging plates were therefore used to increase the dynamic range and make it easier to record the characteristic diffuse distribution, as shown in the EDPs of Fig. 6 (except for Fig. 6d which was recorded on a conventional negative). Note the presence of a spectacular and highly structured characteristic diffuse intensity distribution. Indexation in Fig. 6 is with respect to the underlying parent structure. (Figure 6b was taken from a specimen which had been heated above the nominal α to β phase transition in a hot stage and then cooled back to room temperature. In agreement with Péraudeau *et al.* (7–9), the satellite reflections did disappear on heating above the α to β phase transition. Not all of the satellite reflections, however, reappeared on cooling back to room temperature (cf. Fig. 6b with Fig. 4a). We attribute this to an exacerbation of electron-beam-induced radiation damage upon temperature cycling.)

As mentioned above, there are significant similarities between this observed diffuse distribution and that typical of the family of substoichiometric transition metal carbides and nitrides (14, 15). In particular, the $\langle 110\rangle$ reciprocal space sections, at least to first order, appear virtually identical while the $\langle 012\rangle$ and $\langle 123\rangle$ sections (cf. Fig. 3 of (15) with Figs. 6a and 6d, respectively) clearly have much in common. On the other hand, there are also significant differences in detail. In the case of the $\langle 012\rangle$ zone axis EDPs of Fig. 6a and 6b, for example, the observed diffuse distributions, while similar, are definitely not identical. The presence of the superlattice reflections has therefore in some way perturbed the underlying diffuse distribution away from cubic symmetry.

In the case of the substoichiometric transition metal carbides, e.g., VC_{1-x}, it has been shown that the underlying origin of the observed diffuse distribution arises from C/vacancy ordering in the octahedra of potential C sites surrounding each V atom (15), specifically a requirement that each V atom be surrounded, as far as possible, by 5 C's rather than 4 or 6, i.e., that the local stoichiometry should be the same as the bulk stoichiometry. By analogy, it seems likely that the observed diffuse distribution in the case of $K_3MoO_3F_3$ might well arise from some sort of similar local crystal chemical requirement—perhaps, for example, a requirement that each Mo (and K) always be surrounded by the same number of O's and F's!? Unfortunately, there has to date been no spectroscopic (NMR, EXAFS, ...) study of the local coordination environments in $K_3MoO_3F_3$ which might shed additional light on this suggested origin for the observed diffuse distribution.

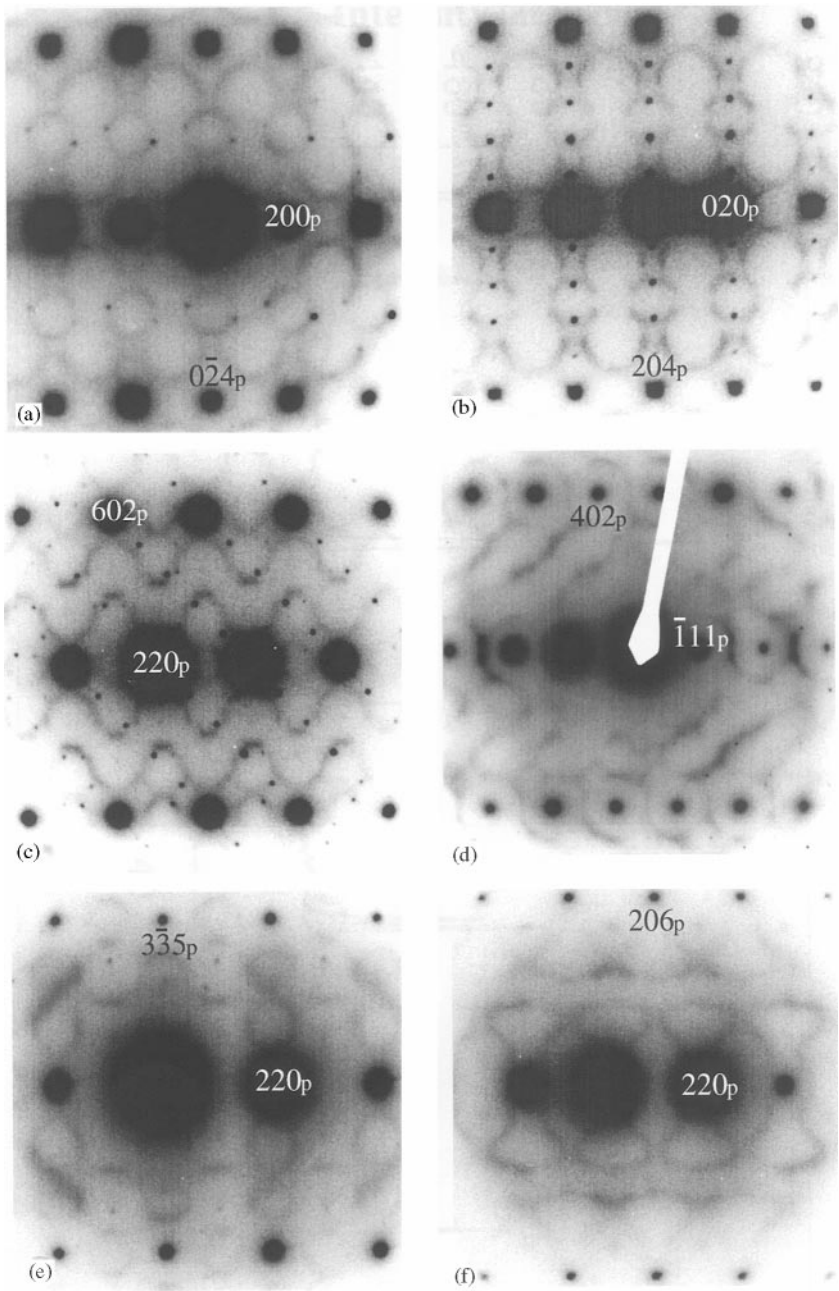

FIG. 6. (a) $\langle 021\rangle_p$, (b) $\langle 20\bar{1}\rangle_p$, (c) $\langle 1\bar{1}3\rangle_p$, (d) $\langle 13\bar{2}\rangle_p$, (e) $\langle \bar{5}56\rangle_p$, and (f) $\langle \bar{3}31\rangle_p$ zone axis EDPs characteristic of the α polymorph of $K_3MoO_3F_3$. Indexation is with respect to the underlying parent structure.

X-Ray Powder Diffraction Results

Figure 7 shows a scanned trace of a room-temperature Guinier pattern of the α polymorph of $K_3MoO_3F_3$ over the 2θ range from 16 to 54°. The parent reflections are shown labelled with the subscript p. Note that relatively few weak nonparent reflections are observed in this 2θ range. Note also that the $\langle 111\rangle_p^*$ and $\langle 222\rangle_p^*$ parent reflections are unsplit whereas the $\langle 002\rangle_p^*$ and $\langle 004\rangle_p^*$ parent reflections are each clearly split into two lines with a rough intensity ration of 1:2, as also are the $\langle 113\rangle_p^*$, $\langle 331\rangle_p^*$, and $\langle 224\rangle_p^*$ parent reflections. (The $\langle 220\rangle_p^*$ parent reflection does not appear to be split in Fig. 7. Inspection of the original Guinier film, however, shows that there are clearly two lines with the weaker of the two lines appearing as a shoulder to high angle in Fig. 7.) These observations are consistent with the earlier observation of Pausewang and Rüdorff (3) that the metric symmetry of the parent structure is tetragonal in

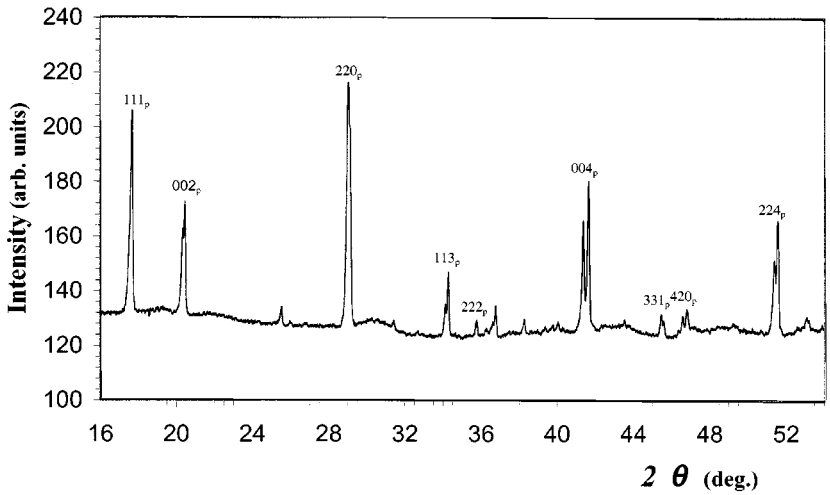

FIG. 7. A scanned trace of a room temperature Guinier pattern of the α polymorph of $K_3MoO_3F_3$ over the 2θ range from 16 to 54°. The parent reflections are shown labelled with the subscript p.

the low-symmetry α polymorph despite the true local symmetry being monoclinic; i.e., a_p^* and b_p^* are accidentally equal despite there being no symmetry requirement for this to be so while c_p^* is ~0.7% smaller.

Refinement of the underlying parent substructure cell dimensions led to lattice parameters given by $a_p = b_p = 8.6653(5)$ and $c_p = 8.7258(8)$ Å. This is in good agreement with the previous results of Paussewang and Rüdorff (3) who gave $a = b = 6.130$ Å ($\equiv a_p = b_p = 6.130\sqrt{2} = 8.669$ Å) and $c = c_p = 8.711$ Å and even with the underlying subcell dimensions given by Peradeau *et al.* (9), i.e., $a_p = b_p = (30.61/5)\sqrt{2} = 8.658$ Å, $c_p = (43.61/5) = 8.722$ Å. Refinement of the resultant monoclinic supercell led to lattice parameters given by $a = 19.403(1)$ Å, $b = 34.661(2)$ Å, and $c = 19.484(1)$ Å with $\beta = 90.318(6)°$.

INTERPRETATION AND CONCLUSIONS

It has been shown that the true symmetry of the low-temperature α polymorph of $K_3MoO_3F_3$ is neither tetragonal, trigonal, nor triclinic as previously reported (3, 4, 6–11) but rather monoclinic $I1a1$, $\mathbf{a} = 2\mathbf{a}_p - \mathbf{c}_p$, $\mathbf{b} = 4\mathbf{b}_p$, $\mathbf{c} = \mathbf{a}_p + 2\mathbf{c}_p$. The nature of the distortion away from the high-symmetry parent structure (see Fig. 1) implied by the existence of the observed satellite reflections is, however, far from clear. Some insight can be obtained from an apparent valence (AV) or bond valence sum calculation (16) using the fractional coordinates (6) reported for the only refined high-temperature parent structure of this general type, i.e., that for $Rb_2KMoO_3F_3$ (see Table 1). The reported fractional coordinates should be closely related to those for $K_3MoO_3F_3$. It can be seen that each O anion is significantly underbonded by approximately twice as much as each F anion is overbonded while each Mo cation is slightly underbonded by an amount similar to that by which each octahedral K cation is overbonded. The interstitial Rb cation is clearly strongly underbonded whatever the O/F distribution of the surrounding anions. The need for structural distortion in order to satisfy more nearly the local crystal chemical requirements of the constituent ions is apparent.

TABLE 1
Bond Valence Sums (AV's) for the Refined Average Structure of $Rb_2KMoO_3F_3$ (6)

Atom	AV	Expected AV
Rb (assuming anions all F)	0.492	1.00
Rb (assuming anions all O)	0.662	1.00
O	1.577	2.00
F	1.183	1.00
Mo (assuming O_3F_3 anions)	5.665	6.00
K (assuming O_3F_3 anions)	1.460	1.00

The much more difficult question to answer is exactly how this happens. The relatively short anion-anion separation distance of ~2.66 Å within the Mo-centered octahedra suggests that they will tend to move as rigid units. By contrast, however, it is by no means necessarily the case that the K-centered octahedra need to rotate as rigid units although many elpasolites do indeed undergo phase transitions primarily associated with octahedral rotation modes (1, 2). In the case of ordinary perovskites, it is well known that octahedral rotation soft modes can only be associated with modulation wave-vectors of $\langle \frac{1}{2}, \frac{1}{2}, \xi \rangle^*$ type. In the case of the (doubled perovskite) elpasolite structure type, the same sort of octahedral rotation soft modes can only be associated with modulation wave-vectors of

$\langle 0, 0, \xi \rangle^*$ type and hence cannot be responsible for the majority of the observed satellite reflections in the case of $K_3MoO_3F_3$. This also rules out a rigid unit mode interpretation for the observed characteristic diffuse intensity distribution.

The fact that at least some of the satellite reflections fall on the observed diffuse distribution suggests that both may well be associated with some form of local O/F ordering and associated structural relaxation. Further "single crystal" diffraction experiments are planned in order to gain insight into the structural distortions responsible.

ACKNOWLEDGMENT

The authors extend their gratitude to SMR Scientific Pty. Ltd. for the temporary use of the Ditabis imaging plate system.

REFERENCES

1. G. Meyer, *Prog. Solid State Chem.* **14,** 141 (1982).
2. I. N. Flerov, M. V. Gorev, K. S. Alexandrov, A. Tressaud, J. Grannec, and M. Couzi, *Mater. Sci. Eng. Rep.* **24,** 81 (1998).
3. G. Pausewang and P. Rüdorff, *Z. Anorg. Allg. Chem.* **364,** 69 (1969).
4. J. Ravez, *J. Phys. III Fr.* **7,** 1129 (1997).
5. P. Hagenmuller, *in* "Perspectives in solid state chemistry" (K. J. Rao, Ed.), pp. 66–78. Narosa, New Delhi, 1995.
6. S. C. Abrahams, J. L. Bernstein, and J. Ravez, *Acta Crystallogr. B* **37,** 1332 (1981).
7. G. Péradeau, J. Ravez, A. Tressaud, P. Hagenmuller, H. Arend, and G. Chanussot, *Solid State Commun.* **23,** 543 (1977).
8. G. Péradeau, J. Ravez, and H. Arend, *Solid State Commun.* **27,** 515 (1978).
9. G. Péradeau, J. Ravez, P. Hagenmuller, and H. Arend, *Solid State Commun.* **27,** 591 (1978).
10. J. Ravez, G. Péradeau, H. Arend, S. C. Abrahams, and P. Hagenmuller, *Ferroelectrics* **26,** 767 (1980).
11. Z. G. Ye, J. Ravez, J.-P. Rivera, J.-P. Chaminade, and H. Schmid, *Ferroelectrics* **124,** 281 (1991).
12. A.-K. Larsson, R. L. Withers, and L. Stenberg, *J. Solid State Chem.* **127,** 222 (1996).
13. R. L. Withers, L. C. Otero-Diaz, and J. G. Thompson, *J. Solid State Chem.* **111,** 283 (1994).
14. J. Billingham, P. S. Bell, and M. H. Lewis, *Acta Crystallogr. A* **28,** 602 (1972).
15. M. Sauvage and E. Parthé, *Acta Crystallogr. A* **28,** 607 (1972).
16. N. E. Brese and M. O'Keeffe, *Acta Crystallogr. B* **47,** 192 (1991).